AGU PUBLICATIONS

JGR

Journal of Geophysical Research: Solid Earth

RESEARCH ARTICLE
10.1002/2017JB014847

On the Grain Size Sensitivity of Olivine Rheology

Chhavi Jain[1], **Jun Korenaga**[1], **and Shun-ichiro Karato**[1]

[1]Department of Geology and Geophysics, Yale University, New Haven, CT, USA

Key Points:
- Published rock deformation data are reanalyzed by a rigorous statistical analysis
- Markov chain Monte Carlo inversion can handle the severe nonlinearity of composite rheology
- The grain size sensitivity of olivine rheology is shown to be poorly constrained by those data

Supporting Information:
- Supporting Information S1

Correspondence to:
C. Jain,
chhavi.jain@yale.edu

Citation:
Jain, C., Korenaga, J., & Karato, S.-I. (2018). On the grain size sensitivity of olivine rheology. *Journal of Geophysical Research: Solid Earth*, *123*, 674–688. https://doi.org/10.1002/2017JB014847

Received 17 AUG 2017
Accepted 26 NOV 2017
Accepted article online 3 DEC 2017
Published online 9 JAN 2018

Abstract Using the Markov chain Monte Carlo (MCMC) inversion technique of Mullet et al. (2015), we reassess the validity of the conventionally accepted values of the grain size exponent of diffusion creep in olivine aggregates. A systematic and comprehensive analysis of individual experimental runs taken from three widely cited studies reveals that these data do not tightly constrain the grain size exponent or any other flow law parameter for diffusion and dislocation creep. Our analysis indicates that large data uncertainties can cause inversion results to deviate significantly from true values because of the covariance between the grain size and stress exponents, and that even resolving a grain size exponent of 2 from 3 is difficult. The versatility of our MCMC inversion technique can, however, be exploited to improve this situation by identifying optimal conditions for future experimental studies. Because the uncertainties of the grain size and stress exponents are highly correlated, for example, increasing the range of grain size variation can help better constrain both exponents simultaneously.

1. Introduction

Under mantle conditions, minerals deform plastically (Karato, 2008). Being volumetrically the most dominant and usually the weakest phase, olivine is believed to control the rheology of the upper mantle (e.g., Goetze & Evans, 1979; Brace & Kohlstedt, 1980; Karato & Wu, 1993; Hirth & Kohlstedt, 2003), and its plastic properties, or flow laws, have been investigated by a number of studies (e.g., Goetze, 1978; Paterson & Chopra, 1981; Karato et al., 1986; Bai et al., 1991; Karato & Wu, 1993; Hirth & Kohlstedt, 1995; Karato & Rubie, 1997; Mei & Kohlstedt, 2000a, 2000b; Faul et al., 2011). Results from these studies have been essential for advancing our understanding of mantle rheology and its role in mantle dynamics (e.g., Solomatov, 1995; Hirth & Kohlstedt, 1996; Korenaga, 2003; Warren & Hirth, 2006; Faul & Jackson, 2007; Kawazoe et al., 2009; Alisic et al., 2012; Boioli et al., 2015).

However, not all flow law parameters reported by the aforementioned studies are in agreement. In particular, their estimates on the grain size exponent for diffusion creep differ appreciably. Theoretical considerations suggest a grain size exponent of 1 for interfacial reaction-controlled mechanism, 2 for diffusional mass transport through the bulk of the crystal, and 3 for diffusion along grain boundaries (e.g., Karato, 2008, chapter 8). Whereas Karato et al. (1986) suggested the grain size exponent of 2 for diffusion creep under dry conditions, for example, Hirth and Kohlstedt (1995) and Mei and Kohlstedt (2000a) obtained an estimate close to 3. Moreover, some studies have suggested a deformation mechanism in which strain rate is not only grain size sensitive but also depends nonlinearly on stress (e.g., Hirth & Kohlstedt, 2003). A range of grain size exponents have been suggested for this mechanism as well: 2 (Hirth & Kohlstedt, 2003), 3 (Faul & Jackson, 2007), 0.7 (Hansen et al., 2011), and 1.1 (Ohuchi et al., 2015).

Given the significance of grain size sensitivity in various aspects of mantle dynamics such as shear localization (e.g., Ricard & Bercovici, 2009) and melt migration (e.g., Cooper & Kohlstedt, 1986), the existing uncertainty of the grain size exponent in the literature is unsettling. In this study, therefore, we revisit deformation data in these experimental studies and aim to understand the source of discrepancy. We restrict ourselves to widely cited "classic" experimental studies, because some results from these studies, such as the grain size exponent of 3, are often incorporated as established facts in the analysis of more recent data (e.g., Faul & Jackson, 2007; Hansen et al., 2011). Because of such historical dependencies, it is important to first evaluate the robustness of experimental constraints brought by the classic data.

In this study, therefore, we use the Markov chain Monte Carlo (MCMC) inversion of Korenaga and Karato (2008) as amended by Mullet et al. (2015) to revisit the studies by Karato et al. (1986), Hirth and Kohlstedt (1995), and Mei and Kohlstedt (2000a, 2000b), with a particular focus on the grain size exponent for diffusion

creep. We will separately analyze data of each study and limit ourselves to the inversion of individual experimental runs for two reasons. First, the conventional values of flow law parameters have been established mostly through the analysis of individual runs. Second, conducting a global inversion requires us to correct for inter-run biases (Korenaga & Karato, 2008), and such an additional layer of complexity could prevent a straightforward comparison with the original studies.

The structure of this paper is as follows. First, we briefly describe the mathematical framework of the MCMC inversion used in this study. We then apply the inversion scheme to experimental data reported in the aforementioned studies and assess the geological implications of our findings. We close by discussing possible future directions to improve our understanding of the rheology of olivine aggregates as a whole.

2. Mathematical Framework

The constitutive equations that govern the steady state deformation of olivine aggregates in the diffusion and dislocation creep regimes are (e.g., Mei & Kohlstedt, 2000a, 2000b; Karato, 2008)

$$\dot{\epsilon}_{\text{diff,dry}} = \dot{\epsilon}_1 = A_1 d^{-p_1} \sigma \exp\left(-\frac{E_1 + PV_1}{RT}\right), \tag{1}$$

$$\dot{\epsilon}_{\text{diff,wet}} = \dot{\epsilon}_2 = A_2 d^{-p_2} C_w^{r_2} \sigma \exp\left(-\frac{E_2 + PV_2}{RT}\right), \tag{2}$$

$$\dot{\epsilon}_{\text{disl,dry}} = \dot{\epsilon}_3 = A_3 \sigma^{n_3} \exp\left(-\frac{E_3 + PV_3}{RT}\right), \tag{3}$$

$$\dot{\epsilon}_{\text{disl,wet}} = \dot{\epsilon}_4 = A_4 \sigma^{n_4} C_w^{r_4} \exp\left(-\frac{E_4 + PV_4}{RT}\right), \tag{4}$$

where $\dot{\epsilon}_i$ is strain rate in s^{-1} due to a certain creep mechanism under either dry or wet conditions, for example, $\dot{\epsilon}_1$ denotes diffusion creep under dry conditions, d is average grain size in microns, σ is deviatoric stress in MPa, P is pressure in Pa, T is absolute temperature in K, C_w is water content in ppm H/Si, R is the gas constant, and A_i is the scaling coefficient for the ith flow law in $s^{-1}MPa^{-n_i}\mu m^{p_i}$. The strain rate in diffusion creep depends on grain size with an exponent p_1 under dry conditions and p_2 under wet conditions. It is assumed to depend linearly on stress (i.e., $n_1 = n_2 = 1$) because nonlinear dependence would be indicative of dislocation-accommodated deformation by grain boundary sliding. Deformation in the dislocation creep regime is independent of grain size (i.e., $p_3 = p_4 = 0$) but varies nonlinearly with stress with an exponent n_3 under dry conditions and n_4 under wet conditions. The strain rate is enhanced by the presence of water in both deformation regimes. Under wet conditions, the strain rate depends on C_w with an exponent r_2 for diffusion creep and r_4 for dislocation creep. The dependence of strain rate on temperature and pressure is characterized by the activation energy E_i and the activation volume V_i, respectively, in the ith deformation mechanism. The above constitutive equations, or flow laws, are valid under the assumption of plastic isotropy.

The quantities P, T, $\dot{\epsilon}$, σ, d, and C_w are state variables and constitute input parameters of our inversion. A total of 18 flow law parameters need to be estimated by inversion: 4 A_i's, 4 E_i's, 4 V_i's, 2 n_i's, 2 p_i's, and 2 r_i's. Whereas all of the state variables can be measured in the laboratory, C_w is often calculated from T and P assuming water saturation (Kohlstedt et al., 1996; Zhao et al., 2004). Determining d is somewhat more involved for two reasons. First, the grain size cannot be measured while a sample is deforming; it is usually measured before the start and at the end of an experiment, and, if the final grain size is bigger than the initial, intermediate grain sizes may be interpolated using the equation of grain growth (Karato, 1989). Second, a polycrystalline sample shows a distribution of grain sizes, and a representative value must be chosen from that distribution. Conventionally, the mean of the distribution is used. This treatment introduces additional uncertainty to the value of d.

Even though each of the constitutive equations (1)–(4) can be linearized by taking the logarithm of the strain rates and may then be handled by the linear least squares approach, a composite flow law provides a more comprehensive framework for experimental deformation data. In this study, deformation is assumed to result from the parallel operation of diffusion and dislocation creep as

$$\dot{\epsilon}_{\text{obs}} = \dot{\epsilon}_{\text{diff}} + \dot{\epsilon}_{\text{disl}}, \tag{5}$$

which represents a highly nonlinear flow law. The MCMC algorithm designed by Korenaga and Karato (2008) can handle nonlinear inversion efficiently. We refer to Korenaga and Karato (2008) for a detailed explanation of the inversion procedure. In this study, we employ their algorithm with some modifications introduced by Mullet et al. (2015). We use the following definition of the misfit or the cost function:

$$\chi_s^2(\{q_k\}) = \sum_{j=1}^{N} \frac{\left(\log \dot{\epsilon}^j_{\text{obs}} - \log \dot{\epsilon}\left(\{q_k\}; \{s_l^j\}\right)\right)^2}{\text{rvar}(\dot{\epsilon}^j)}, \tag{6}$$

where the subscript s is used to denote that we evaluate the simplified cost function defined by Mullet et al. (2015). The superscript j runs through N data points within an experimental run, $\dot{\epsilon}^j_{\text{obs}}$ is the observed strain rate, $\dot{\epsilon}(\{q_k\}; \{s_l^j\})$ is the model prediction using the set of $\{q_k\}$ model parameters at the $\{s_l^j\}$ experimental conditions, and $\text{rvar}(\dot{\epsilon}^j)$ is the relative variance of the observed strain rate, that is, $\text{var}(\dot{\epsilon}^j)/(\dot{\epsilon}^j)^2$. This cost function explicitly considers only the uncertainty of strain rates. The uncertainties of other state variables are implicitly incorporated in our inversion by periodically randomizing those variables within their uncertainties (Mullet et al., 2015).

At the beginning of the MCMC sampling, an a priori range is defined for each model parameter. Whereas Korenaga and Karato (2008) had forced the search for the grain size exponent within the range between 2 and 3 in most of their inversions, we will assume much wider a priori bounds to better understand how the exponent is actually constrained by the chosen deformation data. Our MCMC scheme incorporates the Gibbs sampling to efficiently sample the defined model space by optimizing how to perturb model parameters. Each iteration returns one set of model parameters with a corresponding χ_s^2. The output from all iterations is resampled, typically at every few hundred iterations, to obtain an ensemble of statistically independent model parameters. The a posteriori probability distribution so obtained can then be used to compute various statistical estimators, such as the mean and standard deviation of a model parameter.

The shape of the a posteriori distribution, which is often shown as a histogram, can be used to gauge the nature of the constraints that data impose on a parameter within its a priori bounds. A sharp peak in the distribution indicates tight constraints, whereas the absence of a well-defined peak suggests nonuniqueness in the value of the flow law parameter. Some distributions may show a peak at either end of a priori bounds. In this case, the data may be fit better by a model that lies outside the chosen a priori range, and by using a wider a priori range we can investigate the influence of the bounds. The a posteriori distribution may not always be Gaussian. In this study, we will use the mean and standard deviation as a convenient summary of a posteriori distribution and will discuss the shape of the distribution for a few selected important cases.

3. Reanalysis of Classic Deformation Data

As stated in section 1, we consider individual runs from the following studies: Mei and Kohlstedt (2000a, 2000b, hereinafter referred to as MK00), Hirth and Kohlstedt (1995, HK95), and Karato et al. (1986, KPF86). Runs considered under dry and wet conditions are analyzed separately using the respective composite flow law (equation (5)). We assume wide a priori bounds: $-5 \le p_i \le 5$, $1 \le n_i \le 10$, $-2 \le r_i \le 2$, $10 \le E_i \le 1000$, and $-30 \le V_i \le 30$, where E_i is in kJ mol^{-1} and V_i in cm^3 mol^{-1} (for the influence of the width of a priori bounds on inversion results, see section S1 of the supporting information). As we invert each run separately, we assess only those runs for which the number of data points is greater than or equal to the number of model parameters to be determined. For each data set, we ran 10^6 MCMC iterations, with randomizing data at every 100 iterations and resampling at the interval of 200. The a posteriori probability distributions of model parameters and normalized χ_s^2 (i.e., χ_s^2/N where N is the number of data points) are summarized in Figures 1 and 2.

3.1. Inversion Results

The inversion results for most of dry cases exhibit low p_1 and high n_3 (Figure 1). Many cases are also accompanied with large standard deviations, but the conventional parameter values are often outside the 68% confidence limit ($\pm 1\sigma$). Only run PI-81 of HK95 yields $p_1 \sim 2$–3, which is in agreement with the original published result (cf. Figure 4c of HK95), but the χ_s^2/N for this inversion is large (~10–20), implying possible inconsistencies in data. Incidentally, the largest grain growth occurred in this run; the final grain size (17.6 μm) is a factor of ~2 larger than the initial value (9.6 μm), and the run also contains the largest number of data points (13). These factors could indeed help to constrain p_1 better (section S2).

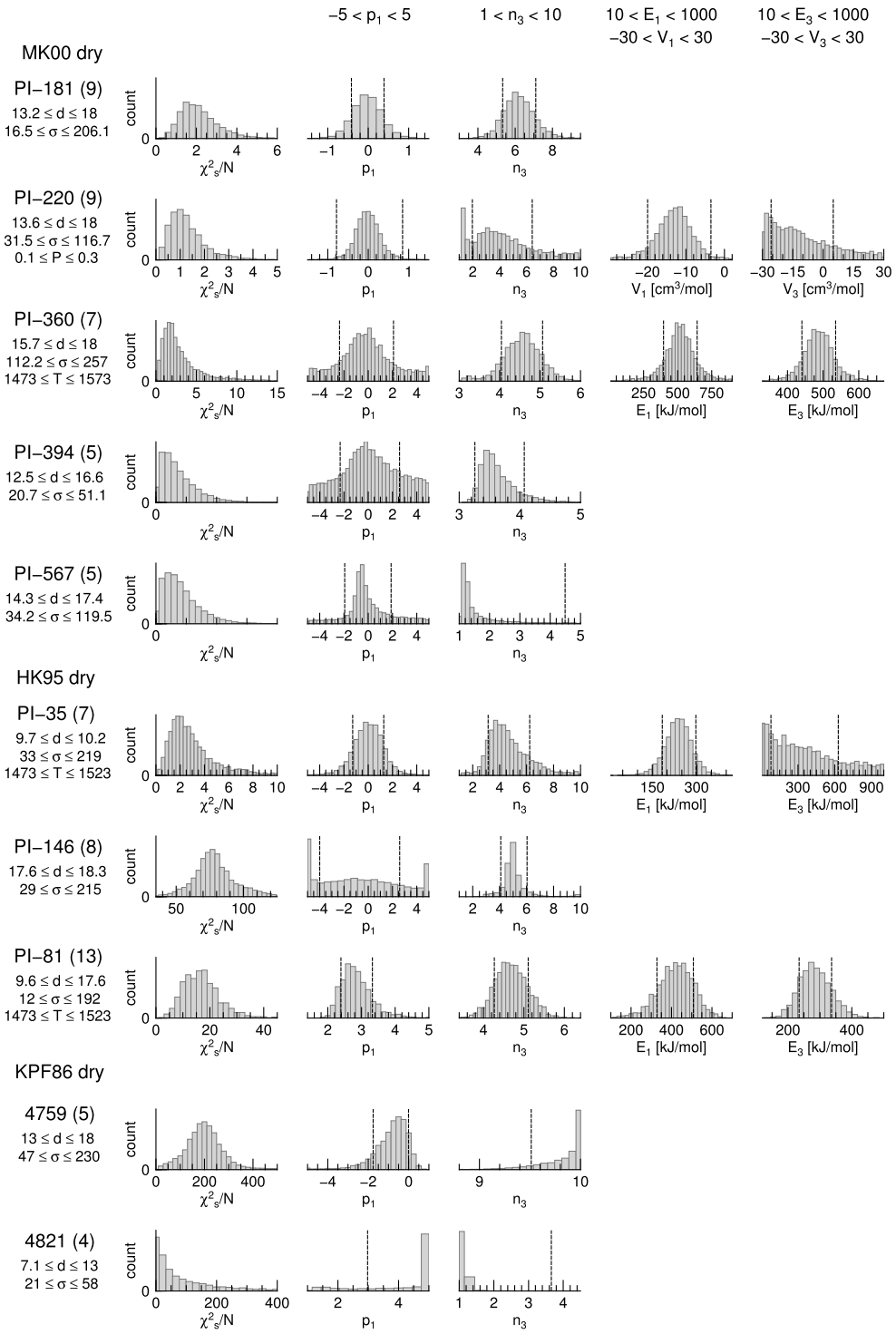

Figure 1. Inversion results of individual experimental runs from Mei and Kohlstedt (2000a, 2000b, MK00), Hirth and Kohlstedt (1995, HK95), and Karato et al. (1986, KPF86) conducted under dry conditions. The a posteriori probability distributions of χ_s^2/N and inverted flow law parameters are shown for each run. The number of data points in a run is denoted in parentheses, and the experimental conditions are also given (d in μm, σ in MPa, T in K, and P in GPa). Each data set is inverted for the composite flow law (equation (5)) with wide a priori bounds (annotated at the top).

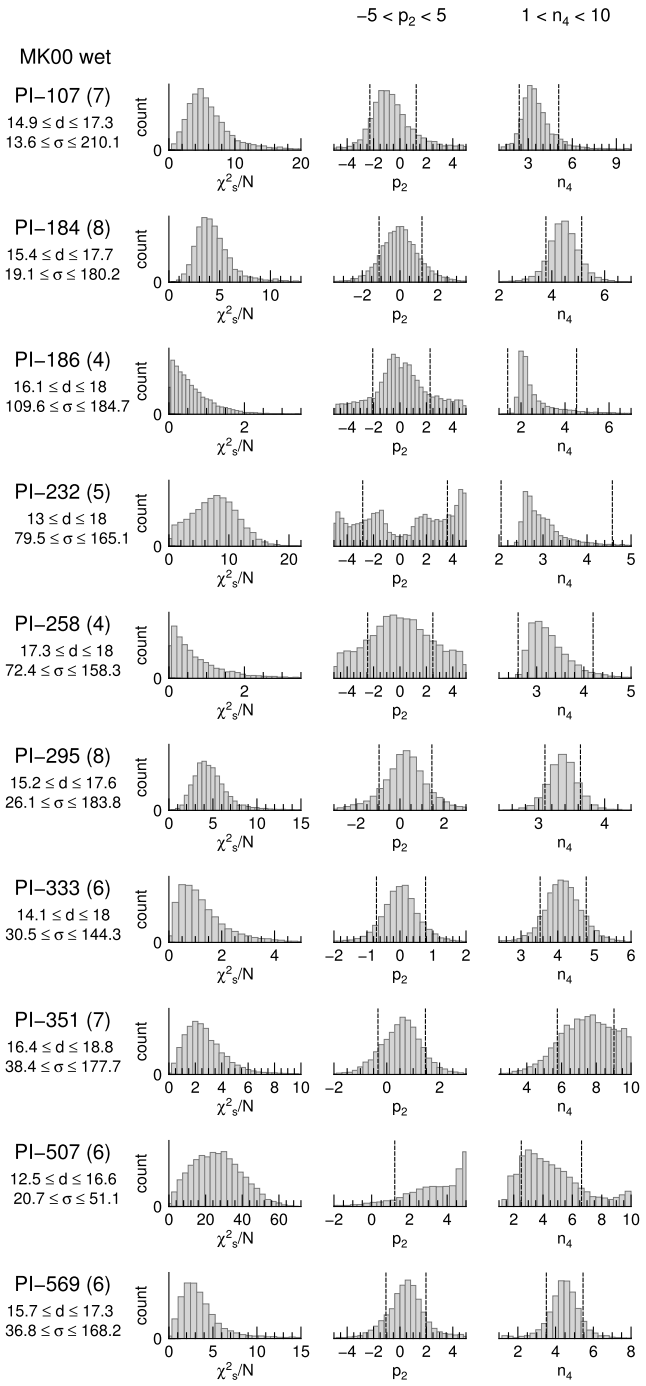

Figure 2. Same as Figure 1 but for runs conducted under wet conditions.

The values of n_3 in most of dry cases are greater than 3. HK95 suggested that data at high stresses in run PI-146 exhibited dislocation creep stress exponent of ~3.5 (Figure 4a of HK95), but this value lies outside one standard deviation associated with our estimate on n_3. In general, our inversion results do not reproduce the grain size and stress exponents originally suggested. In the original studies, the conventional flow law parameters may seem to fit data well, but the practice of assessing model fits after normalizing strain rates to a constant value of stress or grain size can often be misleading. In the case of PI-181, for example, the model fit with conventional exponents appears reasonable (Figures S2a and S2e), but the smallest misfit can instead be achieved with $p_1 \sim 0$ and $n_3 \sim 6$ (Figures S2d and S2h; also compare Figures S1a and S1j). For some dry cases, the uncertainty in the estimated parameters is large enough to include the conventional values (e.g., PI-360, PI-394, and PI-35), so it may be said that these runs are consistent with such conventional values, but they do not tightly constrain the flow law parameters at such values.

Activation energies and volumes are estimated from the few runs that were temperature and pressure variable, respectively. Run PI-35 of HK95 yields $E_1 \sim 246$ kJ mol^{-1} for diffusion creep, which is not very different from the originally published value (315 kJ mol^{-1}), but run PI-81 suggests a much higher E_1 (~418 kJ mol^{-1}). For dislocation creep, run PI-81 returns $E_3 \sim 285$ kJ mol^{-1}, whereas run PI-35 appears to favor a very low E_3. Run PI-360 yields still different estimates on E_1 and E_3, underscoring poorly constrained activation energies for both deformation mechanisms. Run PI-220 of MK00 was the only pressure variable run among all dry cases, and its inversion gives negative V_1 and V_3, inconsistent with the pressure effect expected from theory. This reverse pressure effect is apparent in the raw data of PI-220, for example, the strain rate was 9.0×10^{-7} s^{-1} at the stress of 36.1 MPa under the confining pressure of 100 MPa, whereas a higher strain rate (9.4×10^{-7} s^{-1}) was observed at a lower stress (31.5 MPa) under 300 MPa pressure, indicating that negative activation volumes are not an inversion artifact.

Inversion results for most of wet cases also yield a grain size exponent ~0 or less with large uncertainty (Figure 2), though runs PI-351 and PI-569 return $p_2 \sim 1$. Run PI-507 exhibits stronger grain size dependence ($p_2 > 5$) than the original results of MK00 ($p_2 = 2.8$). Even with the standard linear least squares inversion, we could not reproduce the original result shown in Figure 7 in Mei and Kohlstedt (2000a); notes on these data are, unfortunately, no longer available to identify possible typographical mistakes or other sources of error (S. Mei, personal communication, 2015). Run 4814 of KPF86 showed the largest grain growth, with a factor of ~3 increase in the average grain size (14 μm to 45 μm), and this was the only run to yield p_2 clustering at conventional values. Data misfit is very large for this run, however, suggesting some inconsistencies in data. In contrast, in run 4692, the average grain size remained constant throughout at a large value, so p_2 is not constrained in this case. Given high stresses, samples in this run are likely to have deformed predominantly by dislocation creep, and the inversion yields tight constraints on the stress exponent ($n_4 = 3.31 \pm 0.08$). Many other runs, such as PI-107, PI-186, PI-232, PI-258, and PI-295 of MK00, yield similar mean values of n_4, but the associated uncertainties are large.

Two temperature variable runs in wet cases yield nonoverlapping estimates on the activation energy of diffusion creep E_2: 463 ± 64 kJ mol^{-1} for PI-308 and 328 ± 58 kJ mol^{-1} for PI-568. Our estimates on E_2 from PI-568 (328 ± 58 kJ mol^{-1}) and on E_4 from PI-308 (468 ± 70 kJ mol^{-1}) include the original estimates by MK00 (300 kJ mol^{-1} and 470 kJ mol^{-1}, respectively). However, neither runs could impose meaningful constraints

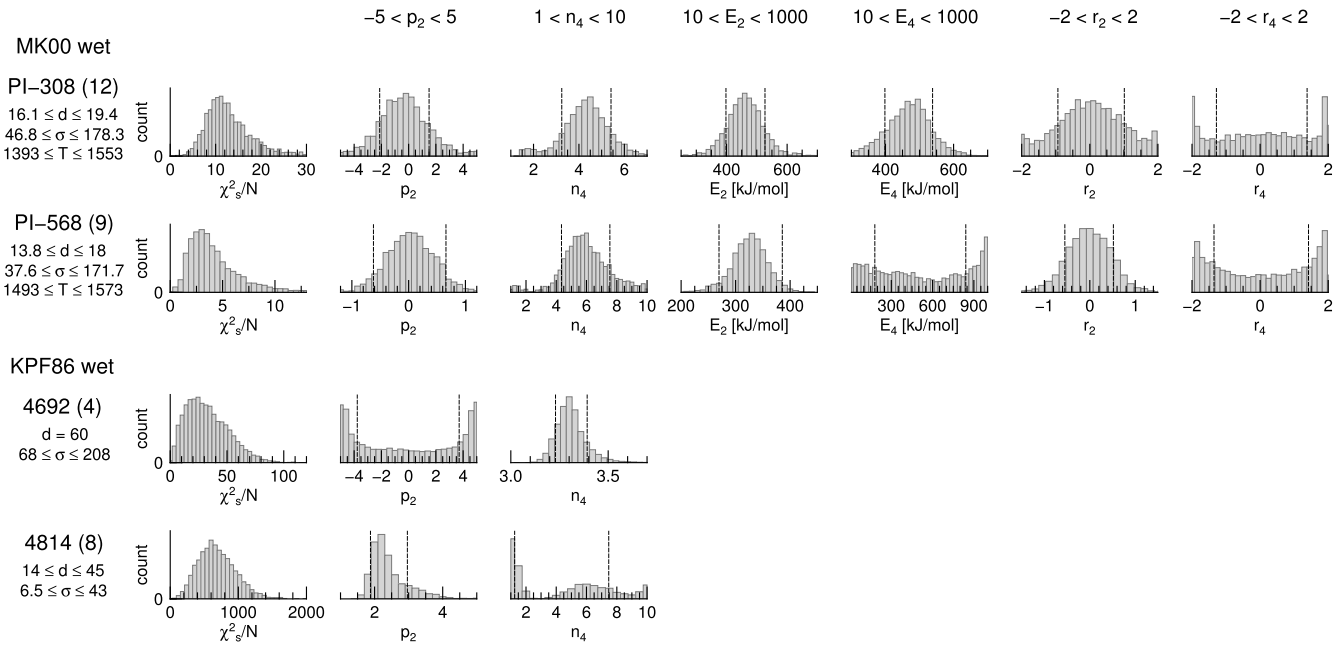

Figure 2. (continued)

on water content exponents r_2 and r_4 probably because water fugacity is more strongly influenced by pressure, which was constant in all the runs that we considered.

In summary, our MCMC inversion shows that the experimental constrains on flow law parameters that can be obtained from these data are of variable quality. For a few cases, our results are consistent with the original published results, for example, runs PI-81 and 4814 could recover the original values of p_1 and p_2, respectively, but the associated uncertainties are too large to resolve the debate over the grain size exponent of diffusion creep. In some cases, original results lie well outside the 68% confidence interval around our mean estimates (e.g., PI-181, PI-220, 4759, and 4821). These results suggest the possibility of greater errors in data than reported. Because variations in grain size are limited in most of experimental runs, it may be obvious for the grain size exponent to be accompanied with large uncertainties, but the conventional value of 3 has been established based on such small variations (Hirth & Kohlstedt, 1995; Mei & Kohlstedt, 2000a). Our estimates on the stress exponent from runs PI−181, PI-360, and PI-569 may also question the validity of the conventional values, given that theoretical considerations provide only loose constraints on this parameter. Also note that the conventional stress exponent of 3.5 suggested by olivine single-crystal deformation data (Bai et al., 1991) has been called into question by the recent reanalysis of the same data (Mullet et al., 2015). Because the classic studies had assumed the conventional values of these exponents to estimate other flow law parameters, our results also question the validity of the activation energies suggested by these studies. The activation energy is typically estimated by fitting a line to data in the strain rate versus $1/T$ space, for which data are normalized to constant grain size and constant stress using the grain size and stress exponents, respectively. The uncertainties of those exponents thus indirectly affect the estimate of activation energy.

For the remaining cases, the original results are included in our estimates because our estimates come with large uncertainties, owing to large errors in data. Such loose a posteriori constraints are, unfortunately, not particularly useful. Inverting multiple runs simultaneously may tighten the constraints. However, different runs place considerably different constraints on flow law parameters (e.g., activation energies), and the quality of these constraints is also variable, so careful data screening will be important. Large χ_s^2 associated with certain results points to inconsistencies in data, and such data may also be excluded. Alternatively, constraints on the grain size exponent may be improved if another grain size sensitive mechanism, that is, grain boundary sliding accommodated by dislocation creep, is included in our composite rheology model. This possibility is explored in the next section.

3.2. Testing the Importance of Grain Boundary Sliding Accommodated by Dislocation Creep

Several studies have suggested the presence of a deformation mechanism for which strain rate is grain size sensitive yet is nonlinearly dependent on stress. Under dry conditions, its flow law may be expressed as

$$\dot{\epsilon}_{\mathrm{gbs,dry}} = \dot{\epsilon_5} = A_5 d^{-p_5} \sigma^{n_5} \exp\left(-\frac{E_5 + PV_5}{RT}\right). \tag{7}$$

This type of flow mechanism is usually attributed to deformation involving dislocation motion associated with grain boundary sliding (GBS) (e.g., Nieh et al., 1997). Deformation maps suggested by Hansen et al. (2011) indicate that GBS dominates in a region between the diffusion-dominated and dislocation-dominated regimes. Under laboratory conditions, therefore, it may operate in parallel with these mechanisms, and its omission in our inversion may have affected our estimates on p_1 and n_3. To consider this possibility, we tested all of the following flow laws:

$$\dot{\epsilon}_{\mathrm{obs}} = \dot{\epsilon}_{\mathrm{gbs,dry}}, \tag{8}$$

$$\dot{\epsilon}_{\mathrm{obs}} = \dot{\epsilon}_{\mathrm{diff,dry}} + \dot{\epsilon}_{\mathrm{gbs,dry}}, \tag{9}$$

$$\dot{\epsilon}_{\mathrm{obs}} = \dot{\epsilon}_{\mathrm{disl,dry}} + \dot{\epsilon}_{\mathrm{gbs,dry}}, \tag{10}$$

$$\dot{\epsilon}_{\mathrm{obs}} = \dot{\epsilon}_{\mathrm{diff,dry}} + \dot{\epsilon}_{\mathrm{disl,dry}} + \dot{\epsilon}_{\mathrm{gbs,dry}}. \tag{11}$$

We used our MCMC algorithm to invert data of a representative dry run, PI-181 of MK00, with each of these models. All inversions were carried out assuming the following wide a priori bounds: from −5 to 5 for the grain size exponents p_1 and p_5, and from 1 to 10 for the stress exponents n_3 and n_5. Because p_1 and n_3 are often assumed to be 3 and 3.5, respectively, we also test the influence of these assumptions on the outcome. Our results are summarized in Table 1, which also includes the inversion results in the previous section for comparison.

Our results (Table 1) indicate that strain rates observed in run PI-181 are best explained by a sum of diffusion and dislocation creep; all models incorporating GBS yield larger misfits. Some of these models are unable to constrain the grain size sensitivity of GBS; the a posteriori probability distribution of p_5 (not shown) for these cases is practically uniform over its a priori range. In most cases, the probability distribution of the stress exponent of GBS shows a second peak at its lower a priori bound, implying that an even lower n_5 may produce a lower χ^2_s. However, justifying a zero, or perhaps a negative, stress exponent of GBS would be unphysical. Additionally, extending the priors for n_5 is unlikely to improve our estimate on p_1, which was found to be constrained near zero irrespective of the a posteriori constraints on other parameters. We may thus conclude that the incorporation of GBS does not bring our estimates on the grain size exponent of diffusion creep closer to its conventionally accepted values. In the remainder of this study, we will therefore not consider this mechanism.

From our MCMC inversion results discussed thus far, the low sensitivity to grain size appears to be a remarkably robust feature of the data from a number of runs. In the next section, we seek to understand the origin of this low sensitivity using various synthetic data sets.

3.3. On the Origin of Low Grain Size Sensitivity

Diffusion creep is expected to dominate when grain size is small because strain rate in this regime is inversely proportional to grain size. Most of our MCMC inversion results (section 3.1), however, show the grain size exponent ~ 0 (albeit with large uncertainties), which implies that diffusion creep could be effective even for larger grains. These results also show that low p_1 is accompanied by n_3 greater than 3, and a combination of these unconventional flow law parameters appears to explain the data better than the conventional values. The origin of the low grain size sensitivity will be investigated in this section by the inversion of synthetic data. In particular, we will focus on the effect of data uncertainties on the inverted model parameters.

We constructed a data set that resembled a typical experimental run; this data set is referred to as S1. We computed strain rates at conditions similar to those reported for run PI-181, using the composite flow law (equation (5)) with the following parameters: $p_1 = 2$ and $A_1 = 2.08 \times 10^{-5}$ for diffusion creep, and $n_3 = 3$ and $A_3 = 1.66 \times 10^{-11}$ for dislocation creep. We assumed $E_1 = V_1 = E_3 = V_3 = 0$ to focus on the estimation of p_1 and n_3. Strain rates were calculated with stresses increasing from 18 to 180 MPa. The average grain size

Table 1
Results of Inversion of Run PI-181 Data of Mei and Kohlstedt (2000a)

Assumed model	Fixed parameters	Inversion results	Misfit (χ_s^2/N)
GBS	–	$p_5 = 0.17 \pm 1.23$, $n_5 = 1.26 \pm 0.15$	18.4
Diffusion+GBS	–	$p_1 = -0.04 \pm 0.48$, $p_5 = -0.002 \pm 2.85$, $n_5 = 6.53 \pm 1.28$	2.20
Diffusion+GBS	$p_1 = 3$	$p_5 = -1.72 \pm 2.01$, $n_5 = 2.39 \pm 0.81$	13.93
Dislocation+GBS	$n_3 = 3.5$	$p_4 = 0.82 \pm 0.74$, $n_4 = 1.04 \pm 0.07$	7.07
Diffusion+Dislocation	–	$p_1 = -0.01 \pm 0.40$, $n_3 = 6.21 \pm 0.89$	1.35
Diffusion + Dislocation + GBS	–	$p_1 = 0.11 \pm 0.80$, $n_3 = 5.25 \pm 2.53$, $p_5 = 0.01 \pm 2.00$, $n_5 = 5.79 \pm 2.25$	37.77
Diffusion + Dislocation + GBS	$p_1 = 3, n_3 = 3.5$	$p_5 = -0.71 \pm 1.97$, $n_5 = 1.27 \pm 0.97$	16.29

Note. The mean values of model parameters are reported, along with their one standard deviations. Normalized misfit is also given. Parameters p_1 and p_5 are the grain size exponents of diffusion creep and dislocation-accommodated grain boundary sliding (GBS), respectively, and n_3 and n_5 are the stress exponents of dislocation creep and GBS, respectively.

was assumed to grow steadily from 13 to 18 μm. To make this data realistic, each variable was associated with the following uncertainty: $\delta\sigma = 2$ MPa, $\delta d = 10\%$, and $\delta\dot{\epsilon} = 5\%$, and the computed strain rates were randomized within their uncertainty bounds. We inverted this data set with wide a priori bounds and obtained $p_1 = 0.97 \pm 0.94$ and $n_3 = 3.18 \pm 0.27$ (Figures 3a and 3c). Similar to our results in section S1, a low grain size sensitivity for diffusion creep is accompanied by a higher stress sensitivity for dislocation creep.

The inversion results yield correlations between various model parameters (Figures 3d–3f), which indicate that, for a model with p_1 lower than 2, n_3 will be greater than 3, the contribution of diffusion creep will be higher, and that of dislocation creep will be lower. Figure 3f also indicates that n_3 is more tightly constrained than p_1. When data uncertainties blur inversion estimates, therefore, p_1 is more easily affected than n_3. The inversion results appear to favor lower values of p_1 and higher values of n_3 with respect to their true values, but despite this shift in the mean values of the flow law exponents, the error ellipse still includes the true model, indicating that the true model produces an acceptably small misfit to data.

A comparison between the strain rates predicted by the true parameters and the mean of MCMC solutions shows that both models can indeed fit the given data reasonably well (Figure 4a). The mean solution corresponds to a greater contribution from diffusion creep, and the predictions from the two models differ mostly at lower stresses and smaller grain sizes, though this difference is small. In contrast, if we look at predicted strain rates from a model with $p_1 > 2$, we find that predictions from the true model and the high-p_1 model appear to agree within reasonable errors at high stresses, where dislocation creep dominates. However, disagreement is observed at small grain sizes and low stresses, where the high-p_1 model predicts much lower contribution of diffusion creep (Figure 4b, inset), and the corresponding misfit is higher. For model predictions to match data in this region, n_3 would have to assume a still lower value, but data at higher stresses would not allow this.

Based on the comparison above, the following explanation seems plausible for the apparent bias toward low p_1 in our inversion results. Data in the dislocation creep regime, that is, at high stresses and large grain sizes, produce relatively tight constraints on n_3. Because the contribution of diffusion creep is negligible here, the value of p_1 does not strongly affect the model fit in this regime. The MCMC inversion therefore samples those

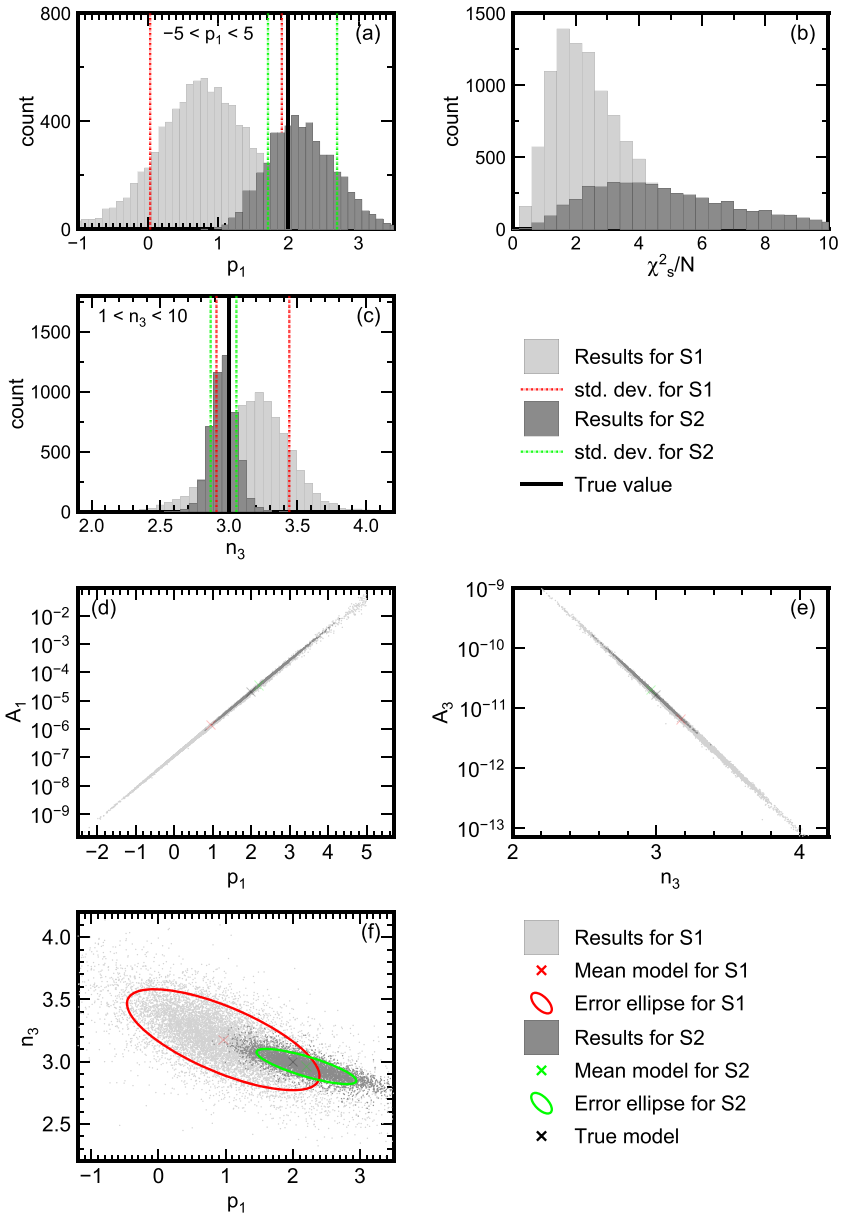

Figure 3. Inversion results with synthetic data. A posteriori probability distribution of (a) p_1, (b) χ_s^2/N, and (c) n_3, obtained from the MCMC inversion of synthetic data sets S1 and S2. Both data sets were constructed using the composite flow law (equation (5)) with the following: $p_1 = 2$ and $A_1 = 2.08 \times 10^{-5}$ for diffusion creep, and $n_3 = 3$ and $A_3 = 1.66 \times 10^{-11}$ for dislocation creep. The two data sets differ only in the uncertainties associated with the state variables. For S1, realistic uncertainties are assumed $\delta\sigma = 2$ MPa, δd = 10%, and $\delta\dot{\epsilon} = 5\%$, whereas S2 is associated with smaller uncertainties $\delta\sigma = 1$ MPa, δd = 1%, and $\delta\dot{\epsilon} = 1\%$. Histograms in light and dark gray show results for inversion of S1 and S2, respectively, and both inversions were conducted with wide a priori bounds. The one standard deviation about the mean estimates on p_1 and n_3 is also marked for S1 (red dotted lines) and S2 (green dotted lines). The true model parameters are represented by a solid black line. Also shown are covariance between (d) p_1 and A_1, (e) n_3 and A_3, and (f) p_1 and n_3, obtained from the inversion of data sets S1 (light gray dots) and S2 (dark gray dots). In Figure 3f, error ellipses (68% confidence zone) are also shown (red for S1 and green for S2), with mean values denoted by crosses. The true model is marked with a black cross.

values of p_1 that can fit strain rates at small grain sizes and low stresses (Figure 4c). We usually expect the true model to produce the best fit to data and other acceptable models to cluster symmetrically around it. But in this data set, as discussed above, models with $p_1 < 2$ can fit data more easily than models with $p_1 > 2$, because low-p_1 models do not require unreasonable values for n_3. Consequently, the probability distribution of the models sampled by the MCMC inversion appears skewed toward low values of p_1 (Figure 4c).

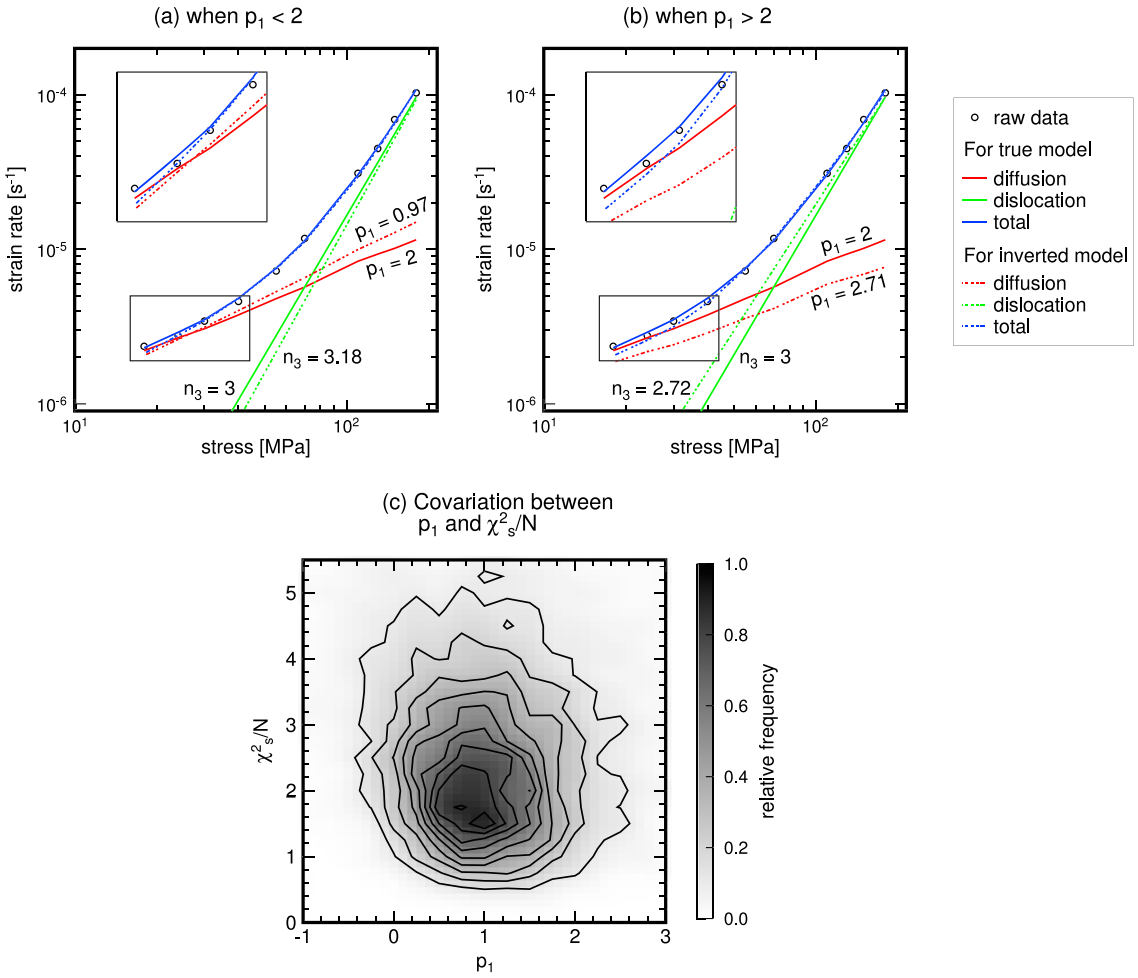

Figure 4. Comparison of the goodness of fit between synthetic data S1 (open circles) and predictions from models with $p_1 < 2$, $p_1 = 2$ (true model), and $p_1 > 2$, in the strain rate versus stress space. Strain rates have not been normalized to a particular grain size, that is, data at low stresses also correspond to smaller grain sizes, and the average grain size increases systematically with stress. (a) Strain rates computed using the true model (solid blue line), that is, $p_1 = 2$ and $A_1 = 2.08 \times 10^{-5}$ for diffusion creep (solid red line), and $n_3 = 3$ and $A_3 = 1.66 \times 10^{-11}$ for dislocation creep (solid green line), are compared with those computed using our mean estimates on the inverted model parameters (blue dotted line): $p_1 = 0.97$ and $A_1 = 1.37 \times 10^{-6}$ for diffusion creep (red dotted line), and $n_3 = 3.18$ and $A_3 = 6.44 \times 10^{-12}$ for dislocation creep (green dotted line). (b) Same as Figure 4a but true model predictions are compared with predictions from a model for which $p_1 > 2$ (blue dotted line): $p_1 = 2.71$ and $A_1 = 1.09 \times 10^{-4}$ for diffusion creep (red dotted line), and $n_3 = 2.72$ and $A_3 = 7.16 \times 10^{-11}$ for dislocation creep (green dotted line). The insets in Figures 4a and 4b zoom in on the model fit in the region of low stresses and small grain sizes. (c) Covariation between p_1 and the corresponding normalized χ_s^2. The gray scale represents relative frequency of samples.

To validate the above reasoning, we synthesized another data set, S2, at conditions identical to S1 using the same model parameters, but with much lower uncertainties: $\delta\sigma = 1$ MPa and $\delta d = \delta\dot{\epsilon} = 1\%$. Its inversion successfully recovered $p_1 \sim 2$ and $n_3 \sim 3$ (Figures 3a–3c). The nature of correlation between different model parameters is the same for S1 and S2 (Figures 3d–3f), but p_1 is more tightly constrained by S2. The error ellipse for S2 in the p_1 versus n_3 space is smaller and nearly symmetric about the true model (Figure 3f), verifying that the bias toward low p_1 seen in the case of S1 indeed results from the uncertainties in data.

Because S1 was synthesized to emulate run PI-181 with respect to the range of experimental conditions and data uncertainties, the reasons discussed above may also explain the low sensitivity to grain sizes obtained for PI-181 and other similar runs (section 3.1). However, unlike the error ellipse for S1 (Figure 3f), the a posteriori probability distribution of p_1 obtained for PI-181 data does not include the conventional values of p_1 within the range of sampled models (Figure S1k). This suggests that experimental data such as those of PI-181 are influenced by errors greater than the reported uncertainties. Such a possibility raises concerns about the reliability of these data sets and their inversion outcome.

The above discussion also underscores the importance of using a composite rheology model. Significant correlation can exist between the flow law parameters for diffusion and dislocation creep mechanisms because both mechanisms must together be able to explain the data that lie in the mixed regime, where diffusion and dislocation creep contribute comparably to the total deformation. Our analysis therefore suggests that, to resolve self-consistent flow law parameters for diffusion and dislocation creep, it is important to analyze deformation data that cover a wide range of experimental conditions and encompass both creep regimes adequately, and such data must then be inverted for a composite rheology. For example, if only high stress data, which seemingly correspond to the dislocation regime only, are inverted for the corresponding flow law parameters, it would likely yield a lower stress exponent than the "true" exponent because the existence of diffusion creep is entirely ignored (e.g., compare blue and green curves in Figure 4a).

4. Discussion and Outlook

Thus far, we have shown that a more comprehensive statistical analysis of laboratory data yields unconventional flow law parameters that nonetheless fit the data more closely than the parameters reported by the original studies. Many of our inversion results in section 3.1 are marginally consistent with the conventional values, but the large uncertainty associated with our estimates makes it difficult to gauge their geophysical relevance. In this section, we will discuss the implications of our inversion results for the study of mantle rheology as well as what can be done to improve our estimates.

4.1. Deformation Maps

Conditions under which materials deform in laboratories are usually very different from those expected in the mantle. For example, geological strain rates are on the order of 10^{-15} s^{-1}, whereas experimental strain rates are 10 orders of magnitude faster (i.e., 10^{-5} s^{-1}). Also, natural samples have larger grains ranging from 0.1 mm to ~10 mm in size as compared to ~10 μm in synthetic samples, and stresses may be of the order of 1 MPa in the mantle, whereas experimental stresses vary between ~10 and 200 MPa. Therefore, applying laboratory findings to understand mantle rheology requires significant extrapolation. We should note that the grain size sensitivity determined for fine-grained samples may not necessarily be the same as the grain size sensitivity in coarse-grained rocks in the actual mantle because grain size sensitivity could be influenced by the change in the rate-controlling diffusion species and diffusion path (e.g., Gordon, 1973; Karato et al., 1986; Karato, 2008, chapter 8). This caveat should always be kept in mind when we visualize the predictions of experimentally determined flow laws under mantle conditions using deformation maps.

The grain size exponent p_1 is one of the key parameters that governs the expanse of the diffusion creep regime, and the importance of constraining this parameter becomes particularly clear by comparing deformation maps that use different values of p_1. Figure 5 shows four deformation maps for dry olivine at 1,523 K and 0.3 GPa, constructed using different sets of flow law parameters for diffusion and dislocation creep. The map drawn using the conventional parameters suggested by Hirth and Kohlstedt (2003, HK03) (Figure 5a), that is, a grain size exponent of 3 and a stress exponent of 3.5 for diffusion and dislocation, respectively, serves as reference. Geologically, 0.3 GPa corresponds to a depth of only ~10 km; our inversion results in the previous section do not constrain activation volumes, so we cannot extrapolate to greater pressures. According to the conventional map, deformation in the shallow upper mantle occurs in the transition region between the two creep regimes, and the effective viscosity at this depth is in the range of $10^{16} - 10^{22}$ Pa s. This range is broadly consistent with other geophysical constraints on upper mantle viscosity, for example, those derived from postglacial rebound (e.g., Mitrovica & Forte, 2004). The Peierls mechanism is ignored here because it is not expected to contribute significantly to the total deformation under these conditions.

Maps drawn using different values of the grain size exponent yielded by experimental data predict distinctly different deformation regimes under the same conditions (Figures 5b–5d). From our MCMC solutions for run PI-360, we choose two models with p_1 close to 2 and 3. Other flow law parameters also differ between these models in accordance with their covariance. Deformation in the shallow mantle may occur entirely in the diffusion creep regime when $p_1 \sim 2$ (Figure 5b), and more importantly, the effective viscosity is different by up to 3 orders of magnitude between Figures 5b and 5c. Figure 5d is based on the mean estimates on flow law parameters for run PI-360 and $p_1 \sim 0$ in this case. Though this solution is consistent with laboratory data, the predicted strain rate for mantle conditions is simply too fast (on the order of 10^{-9} s^{-1}) for the solution to be geologically meaningful.

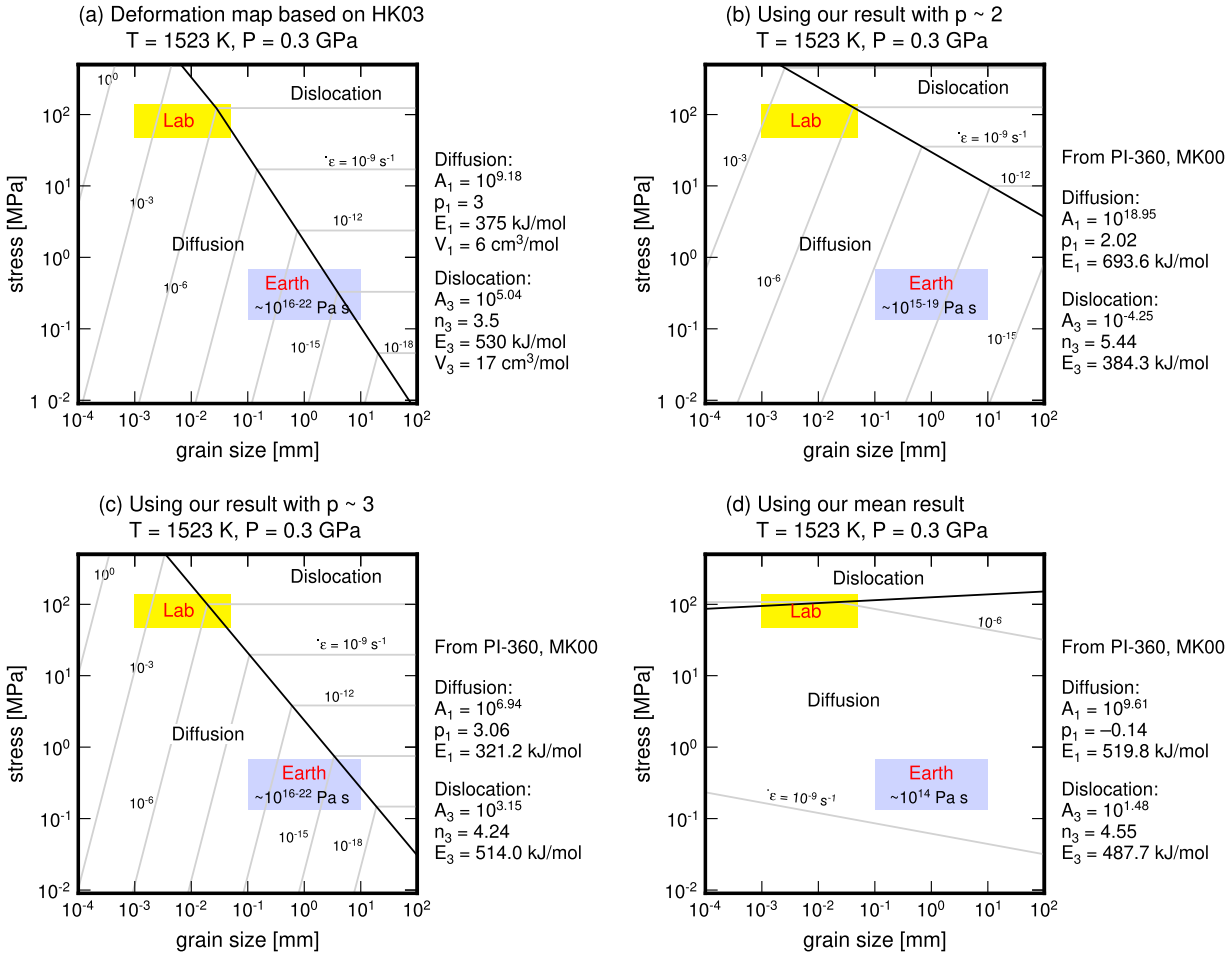

Figure 5. Deformation maps for olivine constructed using a range of values for the grain size exponent (p_1). All maps represent the competition between diffusion and dislocation creep at 1523 K and 0.3 GPa under dry conditions. Constant strain rate contours are drawn in grain size versus stress space. Flow law parameters used to construct each map are mentioned alongside. (a) A reference map drawn using the flow law parameters suggested by Hirth and Kohlstedt (2003, HK03). It is compared with deformation maps drawn using models yielded by the MCMC inversion of run PI-360 of MK00 that fit data reasonably well ($\chi_s^2/N < 1$) but for which (b) $p_1 \sim 2$, (c) $p_1 \sim 3$, and (d) mean estimates on flow law parameters are used. The range of grain sizes and stresses appropriate to the laboratory (yellow rectangle) and to the upper mantle (blue rectangle) is also plotted for each case. The box indicating conditions for Earth also lists the effective viscosity predicted for the upper mantle.

The differences between our results and the reference map underscore the importance of constraining the grain size exponent tightly; due to covariance between flow law parameters, any ambiguity associated with the value of the grain size exponent can propagate to vastly different predictions for mantle rheology. Therefore, the practice of assuming a conventional value for this parameter to make other inferences must be either avoided or supplemented by an assessment of the reliability of those inferences. Also, the activation energies are only loosely constrained, and these uncertainties further affect the deformation regime expected to dominate under upper mantle conditions. Additionally, a wide range of activation volume suggested in the literature could lead to very different deformation maps for deeper mantle. Tightly constraining a whole set of relevant flow law parameters is thus consequential to geodynamical studies.

4.2. Future Directions

To summarize, our MCMC inversion scheme is an efficient way to invert experimental data without making simplifying assumptions about a dominant deformation mechanism. It allows us to analyze data more comprehensively than the standard linear regression technique and fully quantify associated uncertainties. Quantifying uncertainties is essential when assessing the reliability of geophysical applications based on such estimated flow law parameters.

Our reassessment of data from individual runs of some experimental studies shows that the degree to which the flow parameters are constrained depends strongly on the data set that we use, particularly on the range of grain size explored. For example, with the data reported by Mei and Kohlstedt (2000a, 2000b) in which a small range of grain size was explored (13 – 18 μm), the grain size exponent (p) was loosely constrained (with the uncertainty of ±2.5) around a mean value of ~0, which is not consistent with theoretical considerations. In contrast, when we use data sets with a broader grain size range, for example, run 4814 of KPF86 (14–45 μm) and run P-81 of HK95 (9.6–17.6 μm), we obtain more acceptable values ($p = 2.4 \pm 0.5$ for run 4814 and $p = 2.9 \pm 0.5$ for run PI-81). Even with these latter cases, however, we cannot resolve the ambiguity in the grain size exponent, and we may conclude that the commonly assumed value of $p = 3$ (e.g., Drury, 2005; Bürgmann & Dresen, 2008; Skemer et al., 2010; Ohuchi et al., 2015) has very weak experimental support. The poor constraint on the grain size sensitivity also leads to large uncertainties in other flow law parameters. Geodynamical studies should, therefore, take into account the error associated with the mean estimates on flow law parameters and the correlation between various parameters when modeling mantle rheology.

In order to develop a more meaningful geodynamic model of mantle flow, much better constraints on flow law parameters are required, particularly for the diffusion creep regime. A key to improve our understanding of the grain size sensitivity is to obtain better experimental data sets from a broader range of grain size. Our MCMC inversion can be used to investigate optimal conditions to be explored by experimental studies (section S2); because the uncertainties of the grain size and stress exponents are highly correlated, simply widening the range of grain size variation helps to better constrain both exponents. Alternatively, our constraints on flow law parameters may be tightened by "global" inversion, that is, simultaneously inverting data from multiple runs. However, systematic differences among multiple runs would need to be taken into account in such an inversion, adding additional complexity to an already high dimensional nonlinear problem.

Global inversion taking inter-run bias into account was first demonstrated by Korenaga and Karato (2008), and our analysis of single-run data may appear to be a step backward in comparison. However, it was crucial to adopt this more step-wise approach to data analysis for several reasons. First, assessing data from individual runs was important to test the validity of the convention of assuming a grain size exponent of 3, which had been established by inverting the same single-run data (e.g., Hirth & Kohlstedt, 1995; Mei & Kohlstedt, 2000a; Hirth & Kohlstedt, 2003). Second, it offered us a deeper understanding of the nonlinear inversion problem at hand (section 3.3) and highlighted the importance of inverting data that span over a wide range of experimental conditions. It also helped us to suggest ways of improving future experimental design (section S2). Third, the current analysis sets the stage for more complex global inversion. Our investigation of individual experimental runs helped identify erroneous experimental runs that must be excluded from future global inversions.

The deformation of olivine continues to be a subject of active research, and there exist quite a few experimental studies in recent years (e.g., Faul & Jackson, 2007; Kawazoe et al., 2009; Mei et al., 2010; Faul et al., 2011; Hansen et al., 2011, 2012; Ohuchi et al., 2015). Kawazoe et al. (2009) conducted experiments at high pressures to constrain the activation volumes of dislocation creep and the Peierls mechanism, Faul and Jackson (2007) deformed synthetic nearly impurity-free samples over a wide range of grain sizes, and Hansen et al. (2011, 2012) explored a wide range of stress and grain size. These are some of the data sets we can consider next. All of these studies assumed previously published values for some flow law parameters when analyzing their data. Such assumptions can easily be lifted in our MCMC inversion approach. We can also invert multiple runs simultaneously. This would widen the range of experimental conditions being considered and increase the number of data points, both of which should tighten our constraints on flow law parameters (section S2). Our estimates can also be improved with new experimental data, and as discussed in section S2, MCMC inversion can help maximize the resolving power of such new data on flow law parameters.

The output from our MCMC inversion can also be used to carry out a new type of "probabilistic" geodynamical modeling. This modeling approach integrates the findings of rock mechanics into geodynamic simulations by accounting for the nonuniqueness in flow law parameters derived from experimental data. In this approach, the mean and standard deviations of each model parameter, along with covariance among different model parameters, are used to generate a number of flow laws that are consistent with laboratory observations. When applied to the simulation of mantle flow, this ensemble of flow laws will yield a suite of dynamic models that can be compared to relevant geophysical observations such as the spacial distribution of anisotropy estimated from seismic tomography, the depth variation of upper mantle viscosity derived from the study

of postglacial rebound, and the thickness of oceanic lithosphere indicated by the variation of seismic velocity. The subset of dynamic models that agree with such geophysical observations can then be mapped back into the flow law space and tighten the range of acceptable flow law parameters.

By using the Bayesian statistical framework implemented with the MCMC inversion, therefore, not only can we evaluate flow law parameters from existing experimental data but also better understand how experimental rock mechanics and numerical mantle dynamics are actually related. The connection between deformation experiments and numerical simulations, with relevant uncertainties incorporated by probabilistic geodynamical modeling, will facilitate multidisciplinary collaborations among rock mechanics, geodynamics, and seismology.

Acknowledgments
This work was sponsored by the National Science Foundation under grant OCE-1417327. This work was also supported in part by the facilities and staff of the Yale University Faculty of Arts and Sciences High Performance Computing Center. Reviews by Associate Editor Max Moorkamp, Jörg Renner, and an anonymous reviewer were helpful to improve the clarity of the manuscript. All of experimental data analyzed in this study are available in Karato et al. (1986), Hirth and Kohlstedt (1995), and Mei and Kohlstedt (2000a, 2000b), and data uncertainties are tabulated in Korenaga and Karato (2008).

References

Alisic, L., Gurnis, M., Stadler, G., Burstedde, C., & Ghattas, O. (2012). Multi-scale dynamics and rheology of mantle flow with plates. *Journal of Geophysical Research*, *117*, B10402. https://doi.org/10.1029/2012JB009234

Bai, Q., Mackwell, S. J., & Kohlstedt, D. L. (1991). High-temperature creep of olivine single crystals. 1. Mechanical results for buffered samples. *Journal of Geophysical Research*, *96*, 2441–2463.

Boioli, F., Carrez, C., Cordier, P., Devicre, B., & Marquille, M. (2015). Modeling the creep properties of olivine by 2.5-dimensional dislocation dynamics simulations. *Physical Review*, *92*, 014115. https://doi.org/10.1103/PhysRevB.92.014115

Brace, W. F., & Kohlstedt, D. L. (1980). Limits on lithospheric stress imposed by laboratory experiments. *Journal of Geophysical Research*, *85*, 6248–6252.

Bürgmann, R., & Dresen, G. (2008). Rheology of the lower crust and upper mantle: Evidence from rock mechanics, geodesy, and field observations. *Annual Review of Earth and Planetary Sciences*, *36*, 531–567.

Cooper, R. F., & Kohlstedt, D. L. (1986). Rheology and structure of olivine-basalt partial melts. *Journal of Geophysical Research*, *91*(B09), 9315–9323.

Drury, M. R. (2005). Dynamic recrystallization and strain softening of olivine aggregates in the laboratory and the lithosphere, Geological Society, London. *Special Publications*, *243*, 143–158.

Faul, U. H., Fitz Gerald, J. D., Farla, R. J. M., Ahlefeldt, R., & Jackson, I. (2011). Dislocation creep of fine-grained olivine. *Journal of Geophysical Research*, *116*, B01203. https://doi.org/10.1029/2009JB007174

Faul, U. H., & Jackson, I. (2007). Diffusion creep of dry, melt-free olivine. *Journal of Geophysical Research*, *112*, B04204. https://doi.org/10.1029/2006JB004,586

Gordon, R. S. (1973). Mass transport in the diffusion creep of ionic solids. *Journal of the American Ceramic Society*, *56*, 147–152. https://doi.org/10.1111/j.1151-2916.1973.tb15431.x

Goetze, C (1978). The mechanisms of creep in olivine. *Philosophical Transactions of the Royal Society of London A*, *288*, 99–119.

Goetze, C., & Evans, B. (1979). Stress and temperature in the bending lithosphere as constrained by experimental rock mechanics. *Geophysical Journal of the Royal Astronomical Society*, *59*, 463–478.

Hansen, L. N., Zimmerman, M. E., & Kohlstedt, D. L. (2011). Grain boundary sliding in San Carlos olivine: Flow law parameters and crystallographic-preferred orientation. *Journal of Geophysical Research*, *116*, B08201. https://doi.org/10.1029/2011JB008220

Hansen, L. N., Zimmerman, M. E., & Kohlstedt, D. L. (2012). The influence of microstructure on deformation of olivine in the grain-boundary sliding regime. *Journal of Geophysical Research*, *117*, B09201. https://doi.org/10.1029/2012JB009305

Hirth, G., & Kohlstedt, D. L. (1995). Experimental constraints on the dynamics of the partially molten upper mantle: Deformation in the diffusion creep regime. *Journal of Geophysical Research*, *100*, 1981–2001.

Hirth, G., & Kohlstedt, D. L. (1996). Water in the oceanic upper mantle: Implications for rheology, melt extraction and the evolution of the lithosphere. *Earth and Planetary Science Letters*, *144*, 93–108.

Hirth, G., & Kohlstedt, D. L. (2003). Rheology of the upper mantle and the mantle wedge: A view from the experimentalists. In J. Eiler (Ed.), *Inside the Subduction Factory* (pp. 83–105). Washington, DC: American Geophysical Union.

Karato, S.-I. (1989). Grain growth kinetics in olivine aggregates. *Tectonophysics*, *168*, 255–273.

Karato, S.-I. (2008). *Deformation of Earth materials: Introduction to the rheology of the solid Earth*. New York: Cambridge University Press.

Karato, S., & Rubie, D. C. (1997). Towards an experimental study of deep mantle rheology: A new multi anvil sample assembly for deformation studies under high pressure and temperature. *Journal of Geophysical Research*, *102*, 20,111–20,122.

Karato, S., & Wu, P. (1993). Rheology of the upper mantle: A synthesis. *Science*, *260*, 771–778.

Karato, S.-I., Paterson, M., & Fitzgerald, J. D. (1986). Rheology of synthetic olivine aggregates: Influence of grain size and water. *Journal of Geophysical Research*, *91*, 8151–8176.

Kawazoe, T., Karato, S.-I., Otsuka, K., Jing, Z., & Mookherjee, M. (2009). Shear deformation of dry polycrystalline olivine under deep upper mantle conditions using a rotational Drickamer apparatus (RDA). *Physics of the Earth and Planetary Interiors*, *174*, 128–137. https://doi.org/10.1016/j.pepi.2008.06.027

Kohlstedt, D. L., Keppler, H., & Rubie, D. C. (1996). Solubility of water in the α, β and γ phases of $(Mg, Fe)_2SiO_4$. *Contributions to Mineralogy and Petrology*, *123*, 345–357.

Korenaga, J. (2003). Energetics of mantle convection and the fate of fossil heat. *Geophysical Research Letters*, *30*, 1437. https://doi.org/10.1029/2003GL016982

Korenaga, J., & Karato, S.-I. (2008). A new analysis of experimental data on olivine rheology. *Journal of Geophysical Research*, *113*, B02403. https://doi.org/10.1029/2007JB005100

Mei, S., & Kohlstedt, D. L. (2000a). Influence of water on plastic deformation of olivine aggregates. 1. Diffusion creep regime. *Journal of Geophysical Research*, *105*, 21,457–21,469.

Mei, S., & Kohlstedt, D. L. (2000b). Influence of water on plastic deformation of olivine aggregates. 2. Dislocation creep regime. *Journal of Geophysical Research*, *105*, 21471–21481.

Mei, S., Suzuki, A. M., Kohlstedt, D. L., Dixon, N. A., & Durham, W. B. (2010). Experimental constraints on the strength of the lithosphere. *Journal of Geophysical Research*, *115*, B08204. https://doi.org/10.1029/2009JB006873

Mitrovica, J. X., & Forte, A. M. (2004). A new inference of mantle viscosity based upon joint inversion of convection and glacial isostatic adjustment data. *Earth and Planetary Science Letters*, *225*, 177–189.

Mullet, B. G., Korenaga, J., & Karato, S.-I. (2015). Markov chain Monte Carlo inversion for the rheology of olivine single crystals. *Journal of Geophysical Research*, *120*, 3142–3172. https://doi.org/10.1002/2014JB011845

Nieh, T. G., Wang, J. N., Hsiung, L. M., Wadsworth, J., & Sikka, V. (1997). Low temperature superplasticity in a TiAl alloy with a metastable microstructure. *Scripta Materialia*, *37*(6), 773–779.

Ohuchi, T., Kawazoe, T., Higo, Y., Funakoshi, K. I., Suzuki, A., Kikegawa, T., & Irifune, T. (2015). Dislocation-accommodated grain boundary sliding as the major deformation mechanism of olivine in the Earth's upper mantle. *Science Advances*, *1*, e1500360. https://doi.org/10.1126/sciadv.1500360

Paterson, M. S., & Chopra, P. N. (1981). The experimental deformation of dunite. *Tectonophysics*, *78*, 453–473.

Ricard, Y., & Bercovici, D. (2009). A continuum theory of grain size evolution and damage. *Journal of Geophysical Research*, *114*, B01204. https://doi.org/10.1029/2007JB005491

Skemer, P., Warren, J. M., Kelemen, P. B., & Hirth, G. (2010). Microstructural and rheological evolution of a mantle shear zone. *Journal of Petrology*, *51*, 43–53.

Solomatov, V. S. (1995). Scaling of temperature and stress dependent viscosity convection. *Physics of Fluids*, *7*, 266–274. https://doi.org/10.1063/1.868624

Warren, J. M., & Hirth, G. (2006). Grain size sensitive deformation mechanisms in naturally deformed peridotites. *Earth and Planetary Science Letter*, *248*, 438–450.

Zhao, Y.-H., Ginsberg, S. B., & Kohlstedt, D. L. (2004). Solubility of hydrogen in olivine: Dependence on temperature and iron content. *Contributions to Mineralogy and Petrology*, *147*, 155–161.